Novel design strategy for three-channel meta-holography and meta-nanoprinting

Novel design strategy for three-channel meta-holography and meta-nanoprinting

Muhammad Ashar Naveed, Isma Javed, Muhammad Qasim Mehmood, Muhammad Zubair, Yehia Massoud*

Innovative Technologies Laboratories (ITL), King Abdullah University of Science and Technology (KAUST), Saudi Arabia.

ABSTRACT

Multi-functional metasurfaces have gained broad attention recently, as they bring great possibilities for high-dense multi-functional meta-devices, such as projecting holograms and displaying continuous gray-scale images simultaneously. However, currently reported metasurfaces to perform these operations separately. Furthermore, their complex multilayer and super-cell design strategies complicate both design and fabrication processes. This applies a limit on miniaturized, low-cost, integrated multi-functional meta-optics. Here we report a novel single-unit cell-based design strategy to demonstrate a tri-functional metasurface. By merging the spin-decoupling strategy with Mull's law amplitude manipulation, a three-in-one metasurface is designed to project two independent holographic images in the far field and one continuous gray-scale image in the near-field of the metasurface. Specifically, far-field holographic images are projected on orthogonal helicities of white CP light, whereas a near-field image is decoded by creating an orthogonally linearly polarized light path. Furthermore, we optimized a novel gallium phosphide (GaP) material to verify the proposed design strategy for a tri-channel metasurface. The proposed metasurface has high transmission efficiency in the visible regime and verified our design strategy without adding extra complexities to conventional nano-pillar geometry. Therefore, our metasurface opens new avenues in multi-functional meta-device designing and has promising applications in anti-counterfeiting, optical storage, image displays, etc.

Keywords: Tri-channel metasurfaces, Gallium Phosphide, nano-printing, meta-holography.

1. INTRODUCTION

The two-dimensional (2D) planner version of metamaterials, known as metasurfaces, has the exceptional ability to manipulate the electromagnetic (EM) wave through intrinsic properties of amplitude, phase, and polarization [1]–[3]. The subwavelength scale constituent elements offer unprecedented features of EM wave steering, leading to advanced ventures in imagining technology to record high-resolution three-dimensional (3D) holographic objects and nano-printing images with high efficiency [4]–[6]. In recent works, various techniques have been reported to independently control the near-field and far-field wavefront shaping of incident EM waves [7]–[9]. The propagation distance defines these fields, i.e., regions at the subwavelength scale are called near-field, and 3D object reconstruction in this field is often referred to as Fresnel holography [9]–[12]. Whereas regions at propagation distance far beyond the operating wavelength are designated far-field, holography in this region is known as Fourier-type holography [13]–[15]. In order to control both fields simultaneously, the metasurface apportions into segments concerning multiple functionalities [16], stacking multiple layers [17], [18], or interleaving different kinds of nano-resonators [19]–[21] are employed. Although, all aforementioned approaches greatly enhanced the work potential from single to manifolds through hybridizing several unfunctional optical devices that can only modulate a single optical response. Resultantly, light operation for one segment is as noise for other segments of the optical device, leading to efficiency degrading, consistent information density, and inevitable crosstalk.

However, fine-tuning of complex transmission coefficients offers another unique platform for the realization of simultaneous operation of Fourier and Fresnel holography by exploiting dual element-based super-cell coupled response or wave-plates oriented phase delays [22]–[24]. Bao *et al.* have achieved control of far- and near-field by employing the engineering of complex amplitude coefficients based on the inter-element coupling of two nano-resonating antennas [24].In such design strategies, the diffraction efficiency of the far-field Fourier image is degraded by the intensity map of the gray-scale nano-printing image. Propagation and geometric phase mergence along with continuous amplitude engineering are introduced to outplay the constraints of efficiency degradation. This proposed design strategy uses an

*yehia.massoud@kaust.edu.sa

array of nano-resonating antennas with consistent inter-element spacing along with varying geometrical parameters. Though the proposed method has resolved the efficiency constraint, its applicability is greatly dissuaded due to the complex fabrication of varying sizes and dispersion challenges in broadband operation. In addition, primarily reported metasurfaces also suffered significant ohmic losses in the optical regime due to constituent metallic nano-resonators [25], which were overcome by the dielectric metasurface-based silicon, titanium dioxide, and gallium nitride, etc. [26]. Although they have improved their efficiency significantly but still have high aspect ratio challenges. Thus, the simplest design solution that can address all aforementioned design and efficiency challenges is an ultimate demand for technological advancement of multi-functional optical devices.

Here, in the article, we have proposed a unique and simplest design technique that integrates the amplitude modulation directed by Malus's law and helicity-dependent phase decoupling. We used a single nano-resonator of fixed geometrical parameters to encode three distinct holographic information. In order to have high efficiency in large windows of the optical regime, a highly indexed lossless dielectric gallium phosphide (GaP) is utilized. The measured optical constants *"n"* and *"k"* are depicted in Figure 1b. The schematic illustration of the proposed idea is illustrated in Figure 1a. Three selected images of "I," "T" and "L" are decoded in near- and far-field under distinct polarization incidence. When under the incidence of orthogonal components of circularly polarized light, far-field holograms of "I" and "L" are reconstructed, whereas the near-field hologram of "T" is observed through *y*-polarized analyzer under the *x*-polarized incidence.

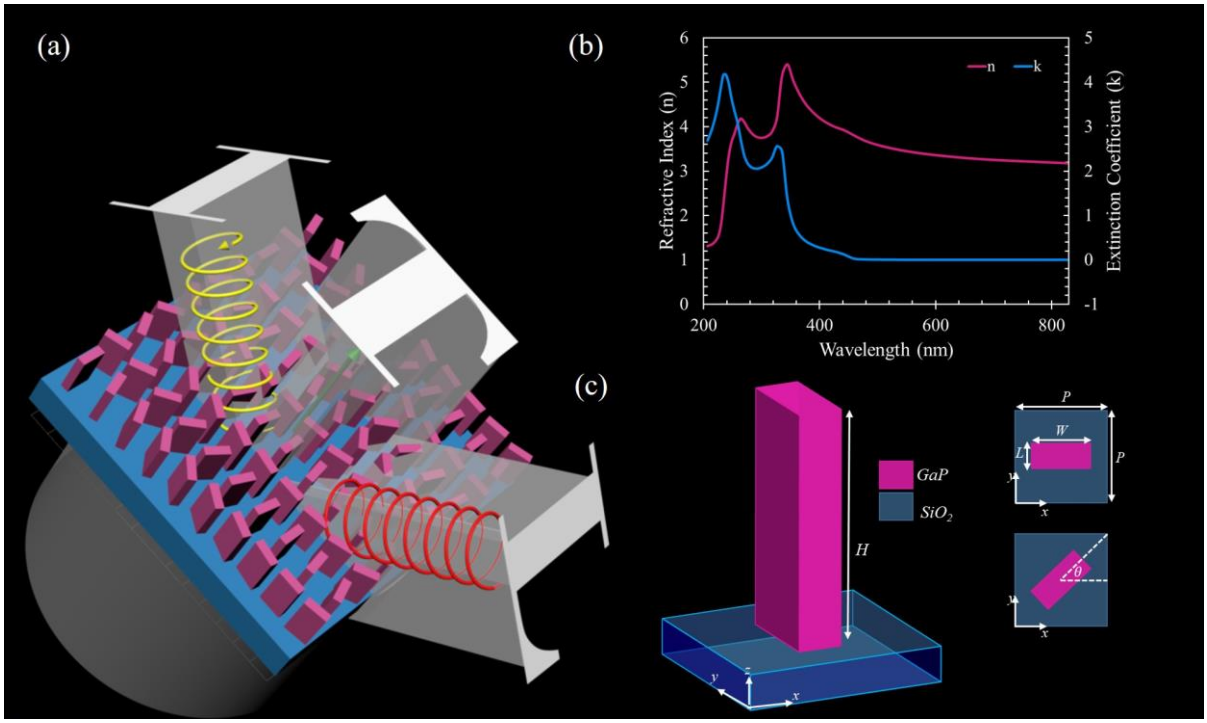

Figure 1. Conceptual illustration of proposed metasurface along with the material properties and unit element. (a) Under the LCP and RCP incident light, the metasurface reconstructs the holographic images of "I" and "L" in far-field, while under linear polarized incidence metasurface produces a holographic image of "T" in near-field analyzed through an orthogonal polarizer. All the holograms are on-axis; for the sake of display ease, they are demonstrated off-axis. (b) Measured optical constants (refractive index and extinction coefficient) of GaP. (c) Schematic depiction of the basic building block, i.e., a nano-pillar constituent of GaP placed over a glass substrate. The optimized geometrical parameters are H=380nm, L=210nm, W=90nm, and P=250nm.

2. METHODOLOGY

2.1 Design Principle

To obtain a tri-channel metasurface, we exploited the geometric phase modulation and amplitude/intensity modulation directed by Malus's law, as demonstrated in Figure 2. Each nano-pillar maximizes the cross-polarized transmitted component and thus has the ability to rotate the spin state. So in the first step, we consider an optical step consisting of an orthogonal linear polarizer to have an amplitude profile for nano-printing. When the metasurface is positioned in this setup, the output intensity distribution can be found as:

$$I(\theta) = I_0 \cdot \sin^2 2\theta \tag{1}$$

where "θ" is in the plane orientation angle of the nano-pillar and "I_0" is the intensity of incident light. Thus, continuous amplitude variation is obtained when we change the *"θ"* from 0^0 to 45^0, as depicted in Figure 3b (blue curve). This enables four possible orientations to generate a binary amplitude modulation scheme. Along with this extra degree of freedom, the spin decoupling strategy can greatly enhance independent, distinct information encoding. The photonic spin hall effect (PSHE) achieves independent control over orthogonal helicities. To do so, Equation 2 is utilized to embed two distinct pieces of information for left circular polarized (LCP) and right circular polarized (RCP).

$$\varphi_m = \arg\left\langle e^{i.\left[\tan^{-1}\left(\tan\left(\frac{\psi_L - \psi_R}{2}\right)\right)\right]} \right\rangle \tag{2}$$

where ψ_L and ψ_R are the phase maps of two distinct information for LCP and RCP, respectively. Thus, the merged profile obtained φ_m from Equation 2 can be decrypted to reconstruct the meta-hologram in far-field.

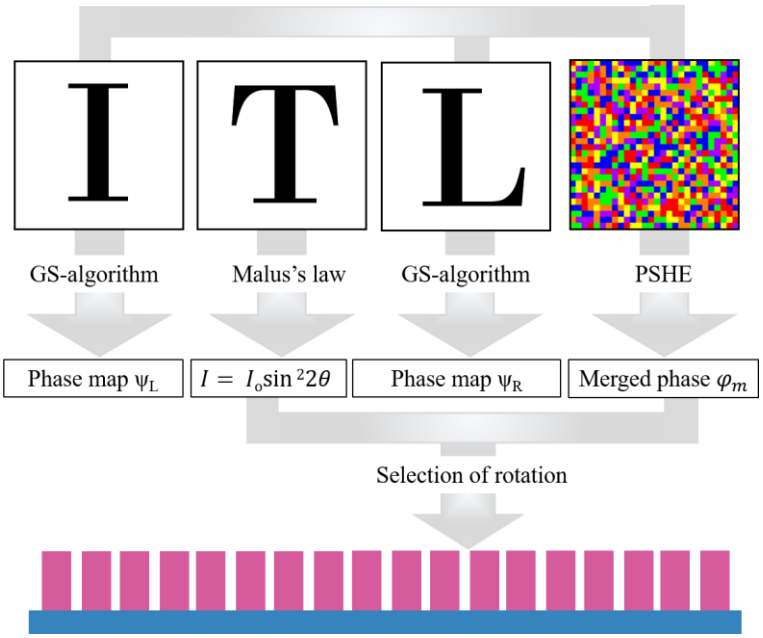

Figure 2. In-depth design principle demonstration of proposed tri-channel metasurface. Initially, phase maps of two selected high-resolution holographic images, "I" and "L" for LCP and RCP, are numerically calculated using the GS algorithm. Then these phase maps are merged through an SOI-based technique (defined by equation 2). Meanwhile, the intensity map of near-field Fresnel hologram "T" is calculated, followed by the discretization of its orientations. Finally, the final phase is imparted on the metasurface by carefully selecting the required orientation angles.

2.2 Unit cell optimization

The subwavelength scale rectangular nano-pillar constituent of gallium phosphide (GaP) placed over a glass substrate is utilized to design the tri-channel optical metasurface. In order to achieve high efficiency, the metasurface design critically depends upon the choice of material for constituent meta-atoms. Thus, to realize a highly efficient optical response, GaP is selected due to its very high refractive index with negligible extinction coefficient in the optical regime, as demonstrated in Figure 1b. Moreover, nano-pillars are optimized to maximize the cross-polarized transmission efficiency to have spin decoupled response for helicity-dependent design. The simulated response of the nano-pillar is depicted in Figure 3a. It can be observed the unit element acts as a half-wave plate by maximizing the cross-polarized component and along with suppressing the co-polarized component in a broad range of the visible spectrum. This optimized unit element is then utilized in metasurface design to realize a highly efficient spin-decoupled response.

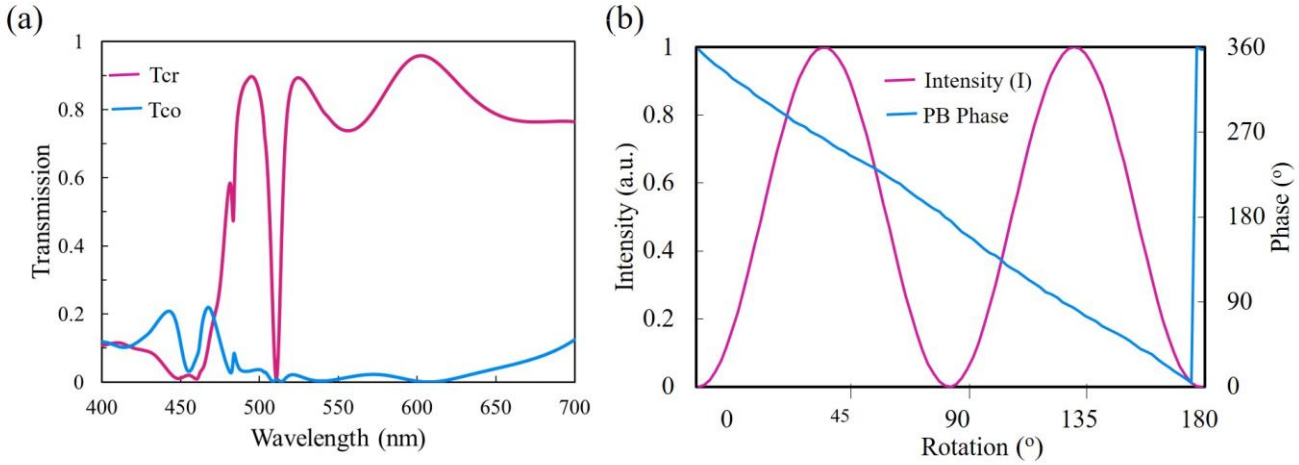

Figure 3. Transmission and phase coverage of optimized nano-pillar. (a) Demonstrate the cross-polarization and co-polarization transmission with pink and blue curves, respectively. (b) Demonstrate the complete phase coverage of 0-2π of nano-pillar along with incessant near-field intensity engineering.

3. RESULTS AND DISCUSSION

To authenticate the proposed design approach for tri-channel metasurface, a 100 × 100 μm^2 metasurface is simulated. In the first step, two images of alphabets "I" and "L" are selected for far-field holography, and then their high-resolution phase mask array of 400 × 400 elements is numerically calculated using GS algorithm. Then these phase masks are merged using Equation 2 for spin-decoupled response realization. On the other hand, the intensity map of the gray-scale image of the alphabet of "T" for 100 × 100 μm^2 metasurface is calculated numerically. Then this intensity profile is mapped into discretized orientation using Equation 1 in four ranges, i.e., θ, $\pi-\theta$, $\pi/2-\theta$, and $\pi/2+\theta$. Afterward, the final phase profile for the tri-channel metasurface is obtained through mapping of merged geometric phase distribution to the nearest available phase choices in 2θ, $\pi-2\theta$, $\pi+2\theta$, and $2\pi-2\theta$ domain. Thus, this method embeds dual information for far-field and single near-field information in a single metasurface. The designed optical metasurface is then simulated using a commercially available EM-solver of lumerical, i.e., finite difference time domain (FDTD) solver. The simulated optical response of the designed metasurface for three distinct wavelengths (488nm, 532nm, and 633nm) under linear and circular polarization is demonstrated in Figure 4. (a1-c1) and (a3-c3) are reconstructed holograms of the alphabet "I" and "L" in far-field under LCP and RCP incidence respectively. Whereas the hologram of the alphabet "T" is observed in the sub-wavelength scaled near-field (just above the metasurface) through the orthogonal linear polarized analyzer (y-polarized) upon horizontally polarized incident light as demonstrated in Figure 4 (a2-c2).

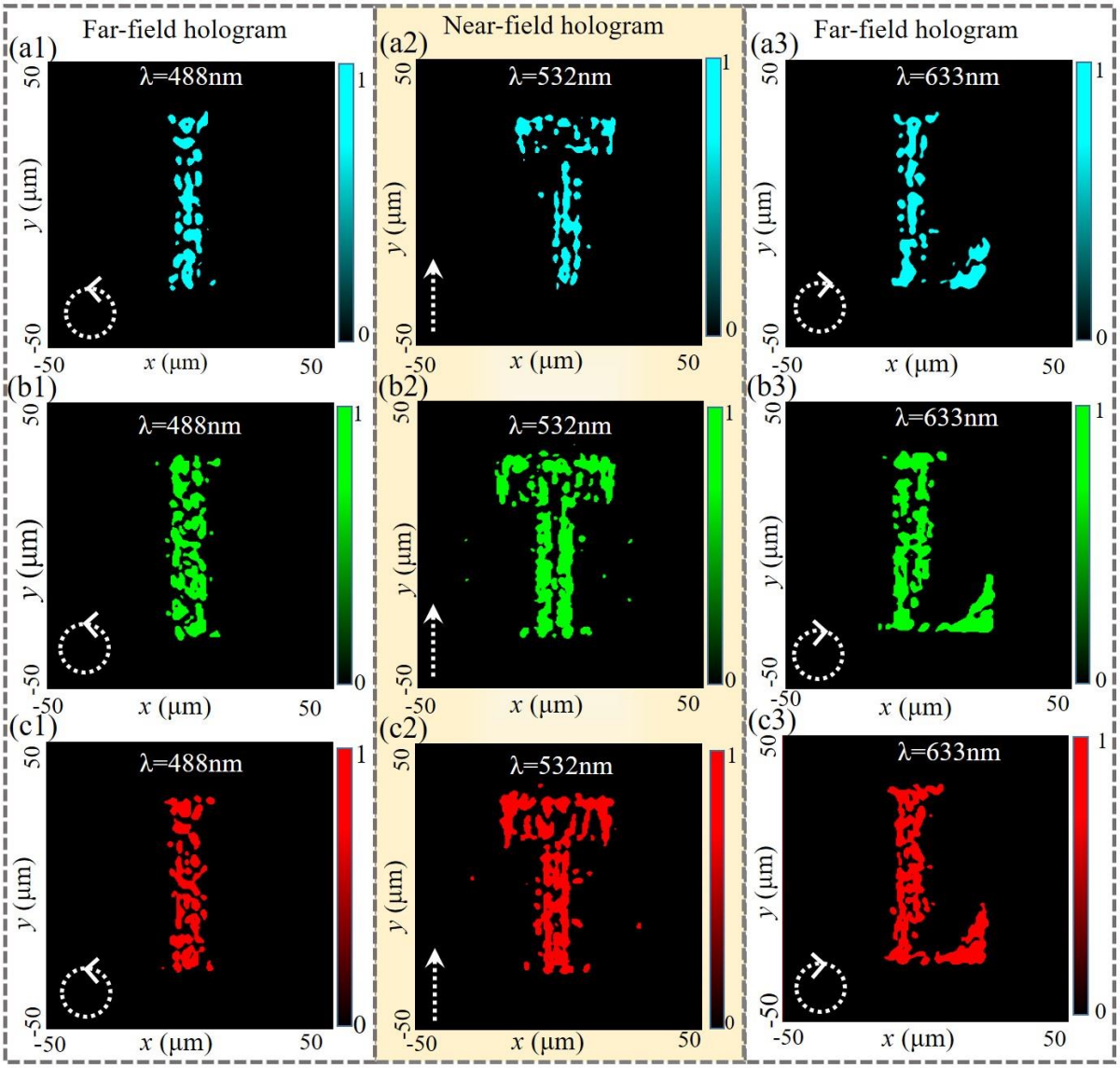

Figure 4. Simulated results of the proposed tri-channel metasurface. Under LCP incidence, the surface reconstructs the meta-hologram of "I" in the far-field, while under LCP illuminance, a hologram of the "L" is observed in the far-field. When linear light is shinned, the Fresnal image of "T" is observed through an orthogonally polarized analyzer in the near field as shown in the yellow highlighted column. (a1-a3) are the simulated results for λ=488 nm, while (b1-b3) and (c1-c3) are the results for λ=532 nm, and λ=633nm respectively.

4. CONCLUSION

In conclusion, we have introduced the simplest and novel design approach for tri-channel multiplexed metasurfaces using a unique combination of Malus's law amplitude manipulation and geometric phase manipulation. In contrast to conventional layer stacking and super cell-based methods, the proposed design exploited a single element-based single-layer all-dielectric metasurface to encrypt the three distinct information. Moreover, a highly indexed lossless material GaP is utilized, and broadband highly efficient response is achieved. The proposed design approach allows a high degree of freedom for independent control of individual channels for data encryption due to the unique mergence of the various optical features tailoring. As a result, dual-channel far-field holography and single-channel near-field nano-printing on

the on-axis symmetric plane is realized. Therefore, the proposed metasurface unlocks new avenues in multi-channel single-layer compact metasurface designing and finds a number of applications in anti-counterfeiting, optical storage, multi-channel displays, etc.

REFERENCES

[1] L. Huang *et al.*, "Dispersionless phase discontinuities for controlling light propagation," *Nano Lett.*, vol. 12, no. 11, pp. 5750–5755, 2012, doi: 10.1021/nl303031j.

[2] N. Yu and F. Capasso, "Flat optics with designer metasurfaces," *Nat. Mater.*, vol. 13, no. 2, pp. 139–150, 2014, doi: 10.1038/nmat3839.

[3] M. Khorasaninejad *et al.*, "Polarization-Insensitive Metalenses at Visible Wavelengths," *Nano Lett.*, vol. 16, no. 11, pp. 7229–7234, 2016, doi: 10.1021/acs.nanolett.6b03626.

[4] M. A. Abbas *et al.*, "Nanostructured chromium-based broadband absorbers and emitters to realize thermally stable solar thermophotovoltaic systems," *Nanoscale*, vol. 14, no. 17, pp. 6425–6436, 2022, doi: 10.1039/D1NR08400C.

[5] R. M. H. Bilal, M. A. Saeed, M. A. Naveed, M. Zubair, M. Q. Mehmood, and Y. Massoud, "Nickel-Based High-Bandwidth Nanostructured Metamaterial Absorber for Visible and Infrared Spectrum," *Nanomaterials*, vol. 12, no. 19, pp. 1–13, 2022, doi: 10.3390/nano12193356.

[6] S. P. Rodrigues, S. Lan, L. Kang, Y. Cui, and W. Cai, "Nonlinear Imaging and Spectroscopy of Chiral Metamaterials," *Adv. Mater.*, vol. 26, no. 35, pp. 6157–6162, Sep. 2014, doi: 10.1002/adma.201402293.

[7] D. Lee *et al.*, "Hyperbolic metamaterials: fusing artificial structures to natural 2D materials," *eLight*, vol. 2, no. 1, pp. 1–23, 2022, doi: 10.1186/s43593-021-00008-6.

[8] S. Ijaz, A. S. Rana, Z. Ahmad, M. Zubair, Y. Massoud, and M. Q. Mehmood, "The Dawn of Metadevices: From Contemporary Designs to Exotic Applications," *Adv. Devices Instrum.*, vol. 2022, no. 9861078, pp. 1–24, 2022, doi: 10.34133/2022/9861078.

[9] L. Cong, Y. K. Srivastava, H. Zhang, X. Zhang, J. Han, and R. Singh, "All-optical active THz metasurfaces for ultrafast polarization switching and dynamic beam splitting," *Light Sci. Appl.*, vol. 7, no. 1, p. 28, Jul. 2018, doi: 10.1038/s41377-018-0024-y.

[10] Y. Rivenson, M. A. Shalev, and Z. Zalevsky, "Compressive Fresnel holography approach for high-resolution viewpoint inference," *Opt. Lett.*, vol. 40, no. 23, p. 5606, Dec. 2015, doi: 10.1364/OL.40.005606.

[11] I. Javed *et al.*, "Broad-Band Polarization-Insensitive Metasurface Holography with a Single-Phase Map," *ACS Appl. Mater. Interfaces*, vol. 14, no. 31, pp. 36019–36026, 2022, doi: 10.1021/acsami.2c07960.

[12] M. Q. Mehmood *et al.*, "Single-Cell-Driven Tri-Channel Encryption Meta-Displays," *Adv. Sci.*, vol. 2203962, pp. 1–9, 2022, doi: 10.1002/advs.202203962.

[13] S. A. Alexandrov, T. R. Hillman, T. Gutzler, and D. D. Sampson, "Synthetic Aperture Fourier Holographic Optical Microscopy," *Phys. Rev. Lett.*, vol. 97, no. 16, p. 168102, Oct. 2006, doi: 10.1103/PhysRevLett.97.168102.

[14] S. G. Kalenkov, G. S. Kalenkov, and A. E. Shtanko, "Spectrally-spatial fourier-holography," *Opt. Express*, vol. 21, no. 21, p. 24985, Oct. 2013, doi: 10.1364/OE.21.024985.

[15] M. A. Naveed *et al.*, "Novel Spin-Decoupling Strategy in Liquid Crystal-Integrated Metasurfaces for Interactive Metadisplays," *Adv. Opt. Mater.*, vol. 10, no. 13, pp. 1–9, 2022, doi: 10.1002/adom.202200196.

[16] Q. A. Alsulami, S. Wageh, A. A. Al-Ghamdi, R. M. H. Bilal, and M. A. Saeed, "A Tunable and Wearable Dual-Band Metamaterial Absorber Based on Polyethylene Terephthalate (PET) Substrate for Sensing Applications," *Polymers (Basel).*, vol. 14, no. 21, p. 4503, Oct. 2022, doi: 10.3390/polym14214503.

[17] H. Chen *et al.*, "Ultra-wideband polarization conversion metasurfaces based on multiple plasmon resonances," *J. Appl. Phys.*, vol. 115, no. 15, p. 154504, Apr. 2014, doi: 10.1063/1.4869917.

[18] Y. Cai and K.-D. Xu, "Tunable broadband terahertz absorber based on multilayer graphene-sandwiched plasmonic structure," *Opt. Express*, vol. 26, no. 24, p. 31693, Nov. 2018, doi: 10.1364/OE.26.031693.

[19] R. M. H. Bilal, M. A. Baqir, M. Hameed, S. A. Naqvi, and M. M. Ali, "Triangular metallic ring-shaped broadband polarization-insensitive and wide-angle metamaterial absorber for visible regime," *J. Opt. Soc. Am. A*, vol. 39, no. 1, p. 136, Jan. 2022, doi: 10.1364/JOSAA.444523.

[20] R. M. H. Bilal *et al.*, "Elliptical metallic rings-shaped fractal metamaterial absorber in the visible regime," *Sci. Rep.*, vol. 10, no. 1, p. 14035, Aug. 2020, doi: 10.1038/s41598-020-71032-8.

[21] D. Wang *et al.*, “Switchable Ultrathin Quarter-wave Plate in Terahertz Using Active Phase-change Metasurface,” *Sci. Rep.*, vol. 5, no. 1, p. 15020, Dec. 2015, doi: 10.1038/srep15020.

[22] M. Kenney, J. Grant, Y. D. Shah, I. Escorcia-Carranza, M. Humphreys, and D. R. S. Cumming, “Octave-Spanning Broadband Absorption of Terahertz Light Using Metasurface Fractal-Cross Absorbers,” *ACS Photonics*, vol. 4, no. 10, pp. 2604–2612, Oct. 2017, doi: 10.1021/acsphotonics.7b00906.

[23] Y. Bao, Y. Yu, S. Sun, Y. Chen, Q. Xu, and C. Qiu, “Dielectric metasurface for independent complex-amplitude control of arbitrary two orthogonal states of polarization,” pp. 1–23, 2021.

[24] M. Liu *et al.*, “Multifunctional metasurfaces enabled by simultaneous and independent control of phase and amplitude for orthogonal polarization states,” *Light Sci. Appl.*, vol. 10, no. 1, 2021, doi: 10.1038/s41377-021-00552-3.

[25] N. T. Q. Hoa, P. H. Lam, P. D. Tung, T. S. Tuan, and H. Nguyen, “Numerical Study of a Wide-Angle and Polarization-Insensitive Ultrabroadband Metamaterial Absorber in Visible and Near-Infrared Region,” *IEEE Photonics J.*, vol. 11, no. 1, pp. 1–8, Feb. 2019, doi: 10.1109/JPHOT.2018.2888971.

[26] P. P. Iyer *et al.*, “Unidirectional luminescence from InGaN/GaN quantum-well metasurfaces,” *Nat. Photonics*, vol. 14, no. 9, pp. 543–548, Sep. 2020, doi: 10.1038/s41566-020-0641-x.